frontiers | Frontiers in Marine Science

TYPE Original Research
PUBLISHED 15 November 2024
DOI 10.3389/fmars.2024.1494930

OPEN ACCESS

EDITED BY
Baohong Chen,
Ministry of Natural Resources, China

REVIEWED BY
Yongyu Zhang,
Chinese Academy of Sciences (CAS), China
Zhangxi Hu,
Guangdong Ocean University, China

*CORRESPONDENCE
Wanchun Guan
gwc@wmu.edu.cn
Rodrigo J. Gonçalves
patagoniaplankton@gmail.com

RECEIVED 11 September 2024
ACCEPTED 28 October 2024
PUBLISHED 15 November 2024

CITATION
Zhu Y, Lin Q, Yang Y, Xia Y, Cai H, Feng X, Gonçalves RJ and Guan W (2024) Ocean acidification enhances the tolerance of dinoflagellate *Prorocentrum donghaiense* to nanoplastic-induced oxidative stress by modulating photosynthetic performance. *Front. Mar. Sci.* 11:1494930. doi: 10.3389/fmars.2024.1494930

Ocean acidification enhances the tolerance of dinoflagellate *Prorocentrum donghaiense* to nanoplastic-induced oxidative stress by modulating photosynthetic performance

Yue Zhu[1,2], Qingming Lin[1,2], Yao Yang[1], Yanmei Xia[1,2], Huidi Cai[1,2], Xucong Feng[1,2], Rodrigo J. Gonçalves[3,4]* and Wanchun Guan[1,2]*

[1]Wenzhou Key Laboratory of Sanitary Microbiology, School of Laboratory Medicine and Life Sciences, Wenzhou Medical University, Wenzhou, China, [2]Institute of Marine Science, Wenzhou Medical University, Wenzhou, Zhejiang, China, [3]Laboratorio de Oceanografía Biológica (LOBio), Centro para el Estudio de Sistemas Marinos (CESIMAR), Consejo Nacional de Investigaciones Científicas y Técnicas (CONICET), Puerto Madryn, Argentina, [4]Departamento de Ecología, Universidad de Granada, Granada, Spain

Introduction: The impact of ocean acidification (OA) and nanoplastics (NPs) on harmful algal blooms (HAB) has emerged as a major global concern. However, the combined effects of OA and NPs on the HAB species are poorly understood.

Methods: In this study, dinoflagellate *Prorocentrum donghaiense*, a typical HAB species, was exposed to varying concentrations of NPs (108.15 ± 8.52 nm) (0, 5, 10, and 15 mg L^{-1}) and CO_2 (low CO_2: 417 ppm, pH: 8.00 and high CO_2: 1045 ppm, pH: 7.73) for seven days to investigate the combined effects of OA and NPs.

Results and discussion: The findings revealed that NPs inhibited the growth of *P. donghaiense* by inducing oxidative stress, as indicated by elevated malondialdehyde (MDA) content and decreased carotenoid/chlorophyll-a ratio, even though photochemical efficiency (φ_{P0}, ψ_0, and φ_{E0}), $rETR_{max}$ and α were enhanced in response to NPs stress. However, OA promoted the growth and alleviated the adverse effects of NPs on *P. donghaiense* by increasing photochemical efficiency (φ_{P0}, ψ_0, and φ_{E0}) and energy flux (RC/CS_0, TR_0/CS_0, ET_0/CS_0) and enhancing the antioxidant ability (increased superoxide dismutase, and decreased MDA). *P. donghaiense* showed enhanced tolerance to NPs under simulated OA conditions. These findings enhance our knowledge of the HAB species response to NPs pollution under future OA scenarios.

KEYWORDS

***Prorocentrum donghaiense*, nanoplastics, ocean acidification, photosynthesis, harmful algal blooms**

1 Introduction

Harmful algal blooms (HAB) have emerged as a global concern, posing a threat to ecological equilibrium and public health (Anderson et al., 2012; Gobler, 2020; Hallegraeff et al., 2021; Xiao et al., 2019). Although HAB exhibit diverse trends across various regions (Dai et al., 2023), there has been a discernible global increase in the occurrence of outbreaks caused by anthropogenic climate changes (Kang et al., 2021; Sha et al., 2021) such as ocean acidification (OA) (Gobler, 2020; Riebesell et al., 2018). Recent studies have indicated a global trend in phytoplankton or HAB, characterized by an increase in dinoflagellate abundance and a decrease in diatom abundance, which is attributed to climate change, including ocean acidification, warming, stronger stratification, eutrophication, and even reduced silicate levels (Brandenburg et al., 2019; Taucher et al., 2022; Zhou et al., 2022). Frequent HAB events have been observed in coastal areas of the East China Sea (ECS) (Zhou et al., 2021). Since 2000, there has been a shift in the predominant bloom-causing species within the ECS, transitioning from diatoms (e.g., *Skeletonema costatum*) to dinoflagellates (e.g., *Prorocentrum donghaiense*) (Xiao et al., 2018; Yu et al., 2023; Zhou et al., 2017, 2022). The latter species are typically dominant during HAB events (Xiao et al., 2019; Yu et al., 2023; Zhang et al., 2021). Between 2000 and 2018, 284 P. *donghaiense* bloom episodes occurred in China, covering a surface area of approximately 70,000 km^2 (Lu et al., 2022), which can alter marine ecosystems by diminishing phytoplankton diversity and zooplankton abundance (Lu et al., 2022). Blooms of *P. donghaiense* may become even more frequent in future climate change scenarios (Lu et al., 2022).

In addition to HAB, another global concern is ocean acidification (OA), which is characterized by an increase in pCO_2 and a decline in pH in surface coastal waters (Lian et al., 2022; Qi et al., 2022). Owing to human activities, atmospheric CO_2 levels have increased from 280 ppm before the industrial revolution to approximately 417 ppm in 2021 (Gao et al., 2021). By 2100, CO_2 is projected to reach 1000 ppm (IPCC, 2014), causing a decrease of 0.14 to 0.4 in pH of ocean water (Gattuso et al., 2015). Elevated CO_2 levels are expected to enhance the growth of some HAB species, particularly dinoflagellates (Brandenburg et al., 2019) such as *Akashiwo sanguinea*, *Karenia mikimotoi, Alexandrium minutum*, and *Amphidinium carterae* (Bausch et al., 2019; Lian et al., 2022; Ou et al., 2017; Wang et al., 2019). However, it is important to note that OA effects are species-specific (Raven et al., 2020). The inhibitory effects of OA are also observed on the growth of dinoflagellate species, such as *A. ostenfeldii* and *A. tamarense* (Brandenburg et al., 2019; Guan et al., 2018). The pigment content, antioxidant systems, and photosynthesis of the HAB species are significantly affected by OA. For example, previous studies have found that OA can increase the pigment content in *K. mikimotoi* (Wang et al., 2023c; Zhang et al., 2022b), whereas it decreases the pigment content in *A. sanguinea*, and *A. minutum* (Lian et al., 2022; Ou et al., 2017). Moreover, OA affects antioxidant enzymes, as it promotes catalase (CAT) activity without altering superoxide dismutase (SOD) in *K. mikimotoi* (Zhang et al., 2022b). Conversely, SOD and CAT activities decrease in *Trichodesmium erythraeum* under OA conditions and are correlated with reduced growth (Wu et al., 2021). Chlorophyll fluorescence is an essential indicator of the photosynthetic performance. The maximum electron transfer efficiency ($rETR_{max}$) and maximum photochemical quantum yield (F_v/F_m) are enhanced under OA conditions, which enhance the growth of *K. mikimotoi* after 96 h and *A. sanguinea* after a week of incubation (Ou et al., 2017; Wang et al., 2023c). Previous studies have also demonstrated that OA can synergistically promote the growth of HAB species in conjunction with other environmental factors such as warming and high irradiance (Ou et al., 2017). Further research has found that OA can alleviate the deleterious effects of some abiotic factors on HAB species, such as solar ultraviolet radiation (Chen et al., 2015), hydrogen peroxide (Qin et al., 2023) and heavy metals (CuO) (Wang et al., 2023a). However, Bausch et al. (2019) reported that OA exacerbated the adverse effects of hypoxia on *A. carterae*.

Microplastics (MPs) and nanoplastics (NPs) pollution can potentially endanger aquatic ecosystems (Besseling et al., 2019). MPs (diameter< 5 mm) are ubiquitous in marine environments, with concentrations varying from 10^{-3} to 1 particle L^{-1} in open and coastal waters (Niu et al., 2021) and from 40 to 760,000 particles L^{-1} in polluted areas (Badylak et al., 2021). The concentration of NPs (diameter< 1 μm) (Wan et al., 2018) is expected to be approximately 10^{14} times greater than that observed for MPs, based on the principles of mass conservation (Besseling et al., 2019). Furthermore, NPs are expected to have a greater potential to harm HAB species than MPs because of their smaller size (You et al., 2021). However, the effects of NPs on the HAB species appear to be species-specific (Nam et al., 2022). NPs negatively affect most species, including *A. pacificum*, *A. carterae*, and *Phaeodactylum tricornutum* (Liu et al., 2021; Sendra et al., 2019; Wang et al., 2021). Neutral or positive effects of NPs have also been observed in several species, including *Microcystis aeruginosa* and *Nostoc* spp (Rowenczyk et al., 2021; Wang et al., 2023b). It has been suggested that NPs can induce oxidative stress in HAB species by producing reactive oxygen species (ROS) and inhibiting antioxidant enzymes, such as SOD (Feng et al., 2020; Natarajan et al., 2020), resulting in elevated levels of malondialdehyde (MDA), ultimately resulting in growth inhibition (Wang et al., 2021). However, in the presence of NPs, cells exhibit increased pigment content (Jiao et al., 2022; Liu et al., 2021; Wang et al., 2021) and altered chlorophyll fluorescence by promoting the maximum photochemical quantum yield (F_v/F_m) to maintain internal homeostasis (Jiao et al., 2022). This effect appears to vary by species, as NPs can also inhibit the electron transport rate (ETR) and effective photochemical quantum yield (F_v'/F_m'), thereby suppressing the growth of *P. tricornutum* (Sendra et al., 2019).

According to previous research, it is expected that the effects of NPs on HAB species may be modulated by environmental factors, such as ocean warming (Zhang et al., 2022a). However, few studies have examined the combined effects of OA and NPs on the HAB species. To the best of our knowledge, only two studies have indicated that elevated pCO_2 mitigates the suppressive effects of MPs and encourages the growth of non-HAB species, Chlorophyta *Nannochloropsis oceanica* and *Scenedesmus obliquus* (Ren et al., 2023; Yang et al., 2020). We hypothesized that OA would alleviate

NP-induced oxidative stress in HAB species by modulating their photosynthetic efficiency and antioxidant mechanisms. The present study aimed to investigate the combined effects of OA and NPs on *P. donghaiense* by monitoring changes in chlorophyll fluorescence parameters (OJIP), relative electron transfer rate (rETR), photosynthetic pigments Chlorophyll-a (Chl-a) and carotenoids (Caro), superoxide dismutase (SOD), and malondialdehyde (MDA). This study examined the potential effects of future OA and NPs pollution on the occurrence of HAB dinoflagellates from the perspective of photosynthetic performance.

2 Materials and methods

2.1 Experimental design

To investigate the combined effects of OA and NPs, *P. donghaiense*, pre-acclimated to ambient and OA conditions for 110 generations, was cultured for seven days with simultaneous exposure to 2 factors. One factor was CO_2 (417 and 1045 ppm), while the other was NPs (108.15 ± 8.52 nm) (0, 5, 10, 15 mg L^{-1}), and the combined treatment groups involved the joint exposure of all different levels of CO_2 and NPs. Low CO_2 concentration (LC, 417 ppm) and high CO_2 concentration (HC, 1045 ppm) were represented the ambient air condition and simulated ocean acidification (OA) condition, respectively. Each treatment comprised of three replicates. The responses of *P. donghaiense* were recorded as photosynthetic variables (pigments, rETR, and OJIP parameters) and oxidative stress biomarkers (SOD, MDA, and Caro/Chl-a). The details of the experimental design are provided below.

2.2 Species culture

Dinoflagellate *P. donghaiense* (Strain: PDES) was isolated from coastal waters around Dongtou Island, Zhejiang Province, East China Sea (27°80′N, 121°20′E). Prior to the experiment, *P. donghaiense* was maintained under simulated OA and ambient CO_2 conditions for approximately 110 generations. The pre-acclimation incubation was conducted in 3-L conical flasks inside growth chambers (RXZ-436C-CO_2, Jiangnan, China) with LED illumination (200 µmol photon m^{-2} s^{-1}, 12L:12D). For the 7-d exposure experiments, the pre-acclimated *P. donghaiense* in the exponential phase was diluted to 1 × 10^4 cells mL^{-1} with fresh f/2 medium (Guillard and Ryther, 1962), and incubated at 20°C under LED illumination (200 µmol photon m^{-2} s^{-1}, 12L:12D). Three replicates were maintained for each treatment.

2.3 OA treatment

Low CO_2 concentrations (417 ppm, LC) and high CO_2 concentrations (1045 ppm, HC) were selected to correspond with the current atmospheric pCO_2 (Gao et al., 2021) and the predicted value for 2100 (IPCC, 2014), respectively. To maintain consistent CO_2 concentrations during the experiments, cultures were continuously aerated with two different CO_2 concentrations (LC and HC) through a 0.22 µm cellulose acetate filter (Shanghai Xinya, China) at approximately 300 mL min^{-1}. The levels of CO_2 in the incubators were monitored continuously using portable carbon dioxide meters (77535, AZ, China), and the pH_{NBS} (National Bureau of Standards) of the culture was measured daily with a portable pH meter (PHS-3E, INESA, Shanghai, China). The carbonate system in the culture was assessed by determining the concentrations of dissolved inorganic carbon (DIC), HCO_3^-, CO_3^{2-} and CO_2 from the measured pH and CO_2 concentrations using the CO2SYS software (Lewis and Wallace, 1998) (Table 1).

2.4 NPs treatment

NPs stock solution (Tianjin Big Goose Technology, China) comprised of 2.5% (w/v) pure polystyrene nanospheres with smooth surfaces. The polystyrene nanospheres are highly

TABLE 1 Growth conditions during incubation of *P. donghaiense*, with an overview of carbonate chemistry for combinations of different NPs and CO_2 concentrations (LC or HC, respectively).

Treatments		pCO_2	pH_{NBS}	DIC	HCO_3^-	CO_3^{2-}	CO_2
CO_2	NPs (mg L^{-1})						
LC	0	417.50 ± 19.19^b	7.98 ± 0.08^a	1833.99 ± 388.40^c	1691.61 ± 329.73^b	131.15 ± 59.32^a	11.22 ± 0.57^b
	5	417.50 ± 19.19^b	8.00 ± 0.09^a	1947.14 ± 458.75^c	1787.68 ± 384.96^b	148.27 ± 74.61^a	11.18 ± 0.57^b
	10	417.50 ± 19.19^b	8.00 ± 0.09^a	1939.85 ± 447.59^c	1781.75 ± 376.74^b	146.91 ± 71.69^a	11.19 ± 0.56^b
	15	417.50 ± 19.19^b	8.01 ± 0.09^a	1977.2 ± 504.47^{bc}	1812.51 ± 422.19^b	153.51 ± 83.23^a	11.18 ± 0.55^b
HC	0	1045.00 ± 28.53^a	7.72 ± 0.06^b	2458.85 ± 382.17^{ab}	2335.06 ± 353.24^a	94.94 ± 29.130^a	28.86 ± 0.77^a
	5	1045.00 ± 28.53^a	7.73 ± 0.08^b	2536.22 ± 489.40^a	2405.03 ± 451.40^a	102.39 ± 38.41^a	28.81 ± 0.87^a
	10	1045.00 ± 28.53^a	7.73 ± 0.08^b	2534.91 ± 471.44^a	2403.98 ± 435.91^a	102.13 ± 35.99^a	28.81 ± 0.89^a
	15	1045.00 ± 28.53^a	7.72 ± 0.10^b	2483.13 ± 523.05^a	2355.43 ± 485.58^a	98.81 ± 38.10^a	28.89 ± 0.93^a

The unit of pCO_2 is ppm, and the units of DIC, HCO_3^-, CO_3^{2-} and CO_2 are µmol kg^{-1}. Data are shown as mean ± SD, i.e., the average of 3 daily replicates during the 7-d incubation (n = 3 × 7). One-way ANOVA (LSD test) results among the treatments are indicated by superscript letters, and the different superscripts indicate significant differences ($p < 0.05$).

hydrophobic and were homogeneously dispersed in 10 mL of deionized water, free of chemical additives and functional groups. The average diameter of the NPs was 108.15 ± 8.52 nm, measured using ImageJ software (National Institutes of Health, USA) (Supplementary Figure S2). Prior to the experiment, the NPs solution was mixed on a vortex mixer (XW-80 A, Haimen Kylin Bell, China) for 2 min. Four nominal NPs concentrations were used: 0, 5, 10, and 15 mg L^{-1}, equivalent to approximately 0, 1×10^{13}, 2×10^{13}, and 3×10^{13} particles L^{-1}, respectively. The hydrophobicity of the NPs and the aeration of the culture medium in the experiment allowed the cells and NPs to be distributed homogeneously in the culture.

2.5 Determination of growth

The cell density was determined daily after sampling by counting the cells with a phytoplankton counting chamber (CC-F, Beijing Polytek, China) under a microscope (Eclipse E200MVR, Nikon, Japan). The growth rate (μ) was calculated using the formula: $\mu = \ln (C_7/C_0)/(t_7 - t_0)$, where C_7 and C_0 represent the cell densities (cells mL^{-1}) on days 7 and 0, respectively. The growth inhibition was estimated using the following equation: Inhibition (%) = (1 – T/C) × 100, where C and T are the cell densities in the control and treatment samples, respectively.

2.6 Pigment analysis

At Day 7, a sample (20 mL) from each treatment was filtered through a glass fiber filter (Whatman GF/F, 25 mm diameter, nominal pore 0.7 μm) to quantify chlorophyll-a (Chl-a) and carotenoid (Caro) contents. Pigments were extracted after mixing the filtered cells with 4 mL of pure methanol and stored in darkness for 24 hours at 4°C. Then the mixture was centrifuged at 2000 g for 10 min (TG16A - WS centrifuge, Saitexiangyi, China) and the absorbance of the supernatants was determined using a spectrophotometer (U-3900; Hitachi, Japan). The pigment contents were calculated as follows: Chl-a (μg mL^{-1}) = $16.29 \times A_{665.2} - 8.54 \times A_{652}$ (Porra, 2002); Caro (μg mL^{-1}) = $4 \times A_{480}$ (Strickland and Parsons, 1972), where $A_{665.2}$, A_{652}, and A_{480} are the absorbances at wavelengths of 665.2, 652, and 480 nm, respectively. The pigment content per cell was determined by dividing the pigment concentration by cell density.

2.7 Determination of oxidative stress biomarkers

Approximately 5×10^6 cells from each treatment group were collected on day 7 after 10 min of centrifugation at 3000 × g (Allegra X-12R Centrifuge, Beckman Coulter, USA). The pellet was resuspended in 5 mL of Milli-Q ultrapure water (SYUP-I-60 L; Shenyuan, China) and lysed at 4°C (JN-Mini Pro; JNBIO, China). The supernatant was obtained by centrifugation at 8000 × g for 10 min at 4°C (Allegra 64R Centrifuge, Beckman Coulter, USA) to assess biochemical indicators. The SOD activity and MDA levels were evaluated according to the manufacturer's instructions (Nanjing Jiancheng Bioengineering, China).

2.8 Measurement of relative electron transfer rate

The rapid light-response curve was obtained using a PSI fluorometer (AquaPenC; Photon System Instruments, Czech Republic). Eight different actinic light intensities (0, 10, 20, 50, 150, 300, 600, and 1000 μmol m^{-2} s^{-1}) were applied for 60 s each. After each light intensity, a 0.8-s saturation light pulse (3000 μmol m^{-2} s^{-1}) captured $\Delta F/F'_m$. The rETR was calculated as follows: $rETR = \Delta F/F'_m \times 0.5 \times E$, where 0.5 represents the allocation of 50% of actinic light energy to photosystem II (PSII), E is for actinic light, and $\Delta F/F'_m$ is the photochemical efficiency of PSII. A hyperbolic tangent function was fitted using this equation (Jassby and Platt, 1976): $Y = rETR_{max} \times \tanh(\alpha \times X/rETR_{max})$, where α denotes light energy utilization efficiency and $rETR_{max}$ indicates the maximum relative electron transport rate.

2.9 Detection of chlorophyll fluorescence transient

On day 7, cells (4 mL) from each replicate were allowed to adapt in the dark for 20 min before measurement. The chlorophyll fluorescence transient (OJIP test) was measured using a PSI fluorometer. The fluorometer measures the transition between O-J-I-P steps: O step is at approximately 20 μs where all PSII reaction centers are open; the J step is at approximately 2 ms; the I step is at approximately 20 ms; and the P step is at about 300 ms where all reaction centers are closed, and the fluorescence intensity reaches its maximum (Strasser and Govindjee, 1992). OJIP curves were drawn to obtain more detailed parameters, including F_v/F_m, V_I, V_J, M_0, Area, S_m, φ_{P0}, ψ_0, φ_{E0}, ABS/RC, TR_0/RC, ET_0/RC, DI_0/RC, RC/CS_0, ABS/CS_0, TR_0/CS_0, ET_0/CS_0, DI_0/CS_0, PI_{ABS}. All data were collected in triplicate, and the values were normalized relative to the LC control treatment (without NPs) to determine the heatmap. The physiological meanings and calculation formulas for these parameters are listed in Supplementary Table S1 (Strasser et al., 2000).

2.10 Statistical analysis

Data are presented as the mean ± standard deviation (SD). Each treatment was performed in triplicate. A one-way ANOVA (LSD) was performed to compare the data among the different treatments on day 7. A two-way ANOVA was employed to evaluate the significant differences and interactions between CO_2 and NP concentrations. All statistical analyses were performed using SPSS (version 26.0, SPSS Inc., Chicago, IL, USA), and figures were plotted using GraphPad Prism (version 9.0, San Diego, CA, USA). Statistical significance was set at $p < 0.05$.

3 Results

3.1 Carbonate system

The carbonate system remained stable in each treatment during the 7-day incubation. The pH values in the LC and HC groups were significantly different ($p< 0.05$). In HC, HCO_3^- and CO_2 levels increased by 34.3% and 157.6%, respectively, while CO_3^{2-} decreased by 31.3% compared to those in LC. The carbonate system in the cultures was not affected by different concentrations of NPs in the treatments within the same CO_2 levels (Table 1).

3.2 Growth and pigments

The growth of *P. donghaiense* was significantly inhibited by the NPs, except at 5 mg L^{-1} in HC (Figure 1). NP-induced growth inhibition exhibited a concentration-dependent trend in both LC and HC treatments (Figure 1B). The inhibition induced by NPs was 7.74%, 17.56%, and 34.82% in LC at 5 mg L^{-1}, 10 mg L^{-1}, and 15 mg L^{-1} NPs, respectively. However, HC treatment promoted growth and mitigated the detrimental effects of NPs compared to LC. The lowest NPs concentration (5 mg L^{-1}) did not inhibit the growth in HC treatment (Figure 1A). NP-induced inhibition also decreased to 9.40% (10 mg L^{-1}), 15.94% (15 mg L^{-1}) in HC treatments compared to that in LC (Figure 1B).

In LC treatments, NPs increased the Chl-a (19.11%–55.46%) and the Caro (9.56%–40.19%) contents but decreased the Caro/Chl-a ratio (Figure 2). Compared with LC, HC (without NPs) did not change Chl-a or Caro/Chl-a ratio but decreased Caro (Figure 2). However, Chl-a and Caro were decreased in HC +NPs treatments, especially at higher NPs concentrations (10 and 15 mg L^{-1}) compared to LC (Figures 2A, B), but Caro/Chl-a ratio did not vary (Figure 2C). The two-way ANOVA tests revealed that CO_2 and NPs significantly affected the growth rate (μ), pigments, and CO_2 was the primary influencing factor. The interactive effects of these two factors were evident on μ and pigments (Table 2).

3.3 Oxidative stress biomarkers

Compared with LC treatment, HC (without NPs) did not significantly alter SOD but enhanced MDA levels (Figure 3).

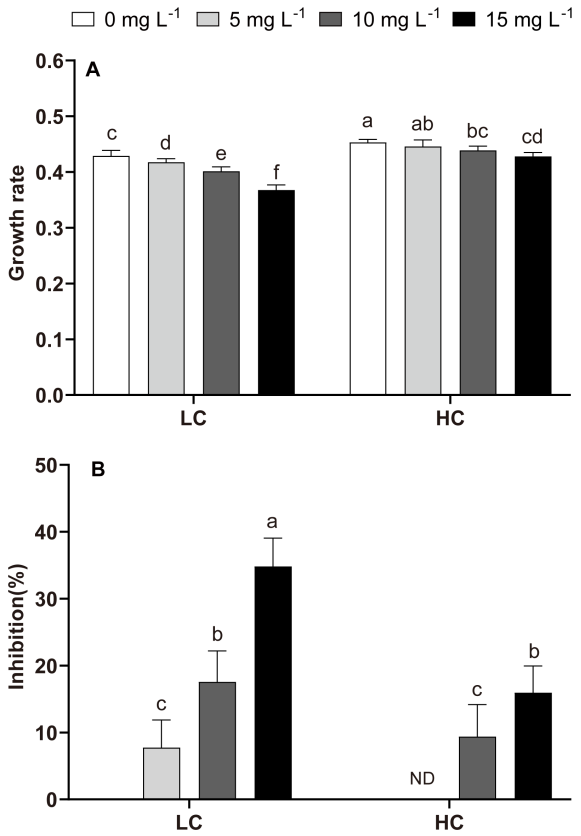

FIGURE 1
Growth rate and inhibition rate of *P. donghaiense* under different NPs and CO_2 treatments at day 7. **(A)**: the growth rate; **(B)**: the inhibition rate. One-way ANOVA (LSD test) results among the treatments are indicated by the letters over the bars and different letters indicate significant differences among treatments ($p< 0.05$). ND: There was no significant difference in inhibition rate between 5 mg L^{-1} NPs at HC and HC (without NPs). Error bars represent the standard deviation of the mean of biological triplicates.

10.3389/fmars.2024.1494930

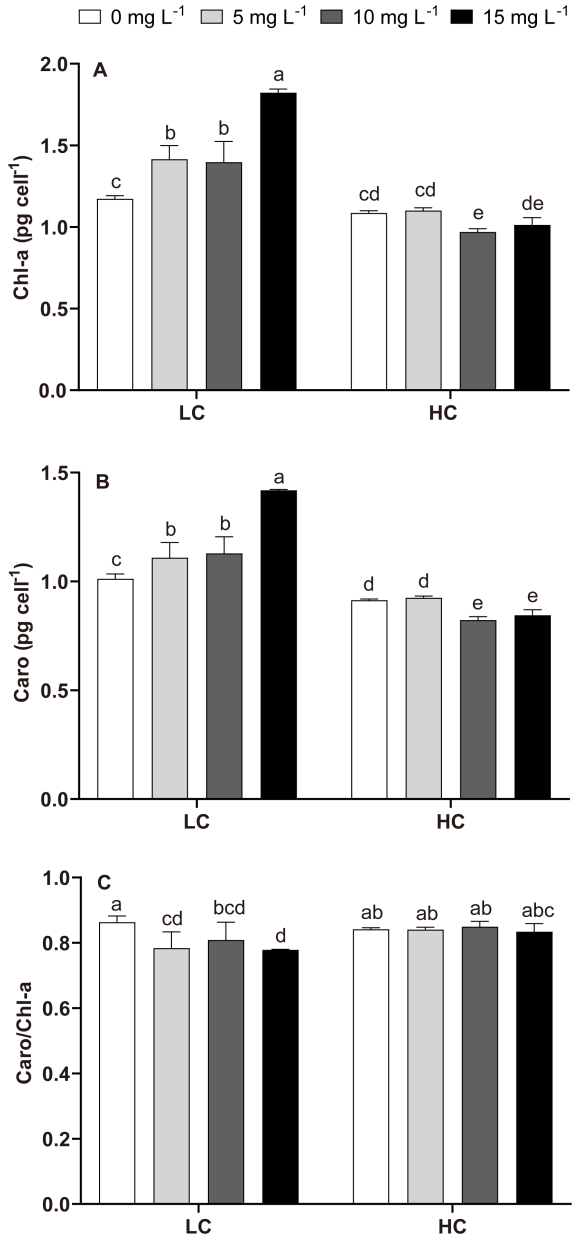

FIGURE 2
Chlorophyll-a (Chl-a), carotenoid (Caro) contents, and Caro/Chl-a ratio of *P. donghaiense* under different NPs and CO_2 treatments at day 7. **(A)** Chl-a, **(B)** Caro, **(C)** Caro/Chl-a. One-way ANOVA (LSD test) results among the treatments are indicated by the letters over the bars and different letters indicate significant differences among treatments ($p < 0.05$). Error bars represent the standard deviation of the mean of biological triplicates.

The effects of NPs on the SOD and MDA levels varied in the LC and HC groups. No significant effect of NPs on SOD was detected in the LC treatment, except in the 5 mg L^{-1} NPs treatment (Figure 3A). High NPs concentration (15 mg L^{-1}) significantly increased the MDA content in LC-treated cells (Figure 3B). Compared to LC, HC +NPs treatment enhanced SOD activity but reduced MDA content (Figure 3). The two-way ANOVA tests revealed that SOD and MDA levels were significantly affected by CO_2 and NPs, with CO_2 being the major influencing factor. Moreover, the interactive effects of CO_2 and NPs on the SOD and MDA levels were also evident (Table 2).

3.4 The response of rETR

The rapid light curves and photo-physiological parameters (α, $rETR_{max}$, and E_k) revealed the responses of *P. donghaiense* to different treatments (Figure 4). Compared to LC treatment, HC, LC+NPs, and HC+NPs significantly enhanced the slope of the rETR curve (α), the maximum electron transport rate ($rETR_{max}$) and the light saturation point (E_k) (Table 3). However, HC+NPs did not further enhance these three parameters compared with HC (without NPs) (Table 3). The two-way ANOVA tests revealed that CO_2 significantly affected α, while NPs significantly affected

10.3389/fmars.2024.1494930

TABLE 2 Significance of growth rate (μ), chlorophyll-a (Chl-a), carotenoid (Caro), Caro/Chl-a, superoxide dismutase (SOD), malondialdehyde (MDA), reactive oxygen species (ROS), the maximum relative electron transfer rate ($rETR_{max}$), the initial slope of the RLC (α), and $rETR_{max}/\alpha$ (E_k) of *P. donghaiense* under different CO_2 and NPs concentrations, as reported from two-way ANOVA.

Source of variation		μ	Chl-a	Caro	Caro/ Chl-a	SOD	MDA	$rETR_{max}$	α	E_k
CO_2	F	200.76	298.570	332.752	7.684	144.118	25.376	1.413	30.716	0.561
NPs		48.92	28.017	23.203	3.022	5.558	3.541	30.389	28.820	13.550
CO_2 × NPs		9.34	40.608	42.254	2.441	14.364	24.660	20.782	28.070	8.241
CO_2	p	<0.001	<0.001	<0.001	0.014	<0.001	<0.001	0.252	<0.001	0.465
NPs		<0.001	<0.001	<0.001	0.060	0.008	0.039	<0.001	<0.001	<0.001
CO_2 × NPs		<0.001	<0.001	<0.001	0.102	<0.001	<0.001	<0.001	<0.001	0.002

"F" is the statistic and "p" is the p value, and the statistical significance is considered when $p < 0.05$.

$rETR_{max}$, α, and E_k. Additionally, an interactive effect between these two factors on $rETR_{max}$, α, and E_k was observed (Table 2).

3.5 The response of the OJIP curve and parameters

The chlorophyll fluorescence intensity transitions from its minimum level (O-level) to its maximum level (P-level) through two intermediate steps, designated J and I (Supplementary Figure S3). The OJIP curve's slope increased significantly when exposed to NPs under LC conditions, indicating that the reduction of Q_A was faster (Supplementary Figure S3A). The slope change was significantly less in *P. donghaiense* cultures that were exposed to NPs under HC treatments (Supplementary Figure S3B).

The response mechanisms of cells to HC, NPs, and HC+NPs treatments were revealed when the relevant parameters were

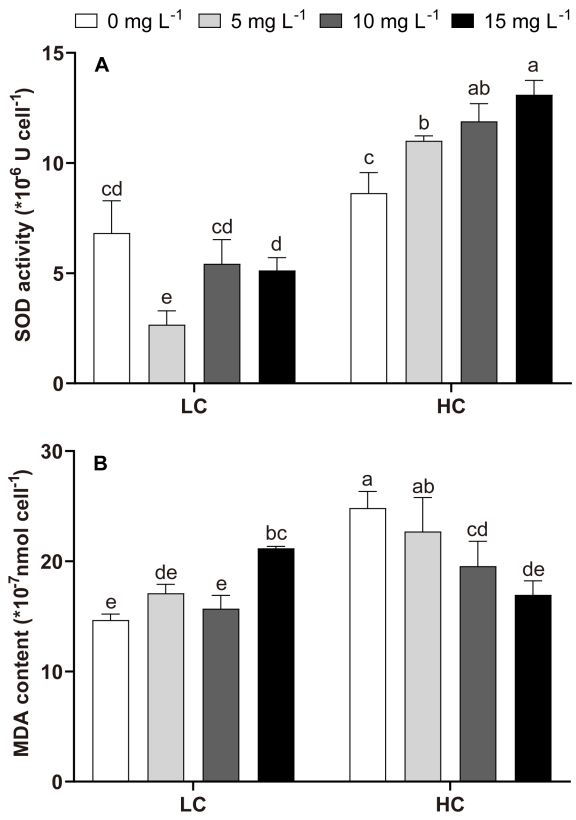

FIGURE 3
Biochemical indicators of *P. donghaiense* related to oxidative stress under different NPs and CO_2 treatments at day 7. **(A)**: SOD activity; **(B)**: MDA content. One-way ANOVA (LSD test) results among the treatments are indicated by the letters over the bars and different letters indicate significant differences among treatments ($p < 0.05$). Error bars represent the standard deviation of the mean of biological triplicates.

10.3389/fmars.2024.1494930

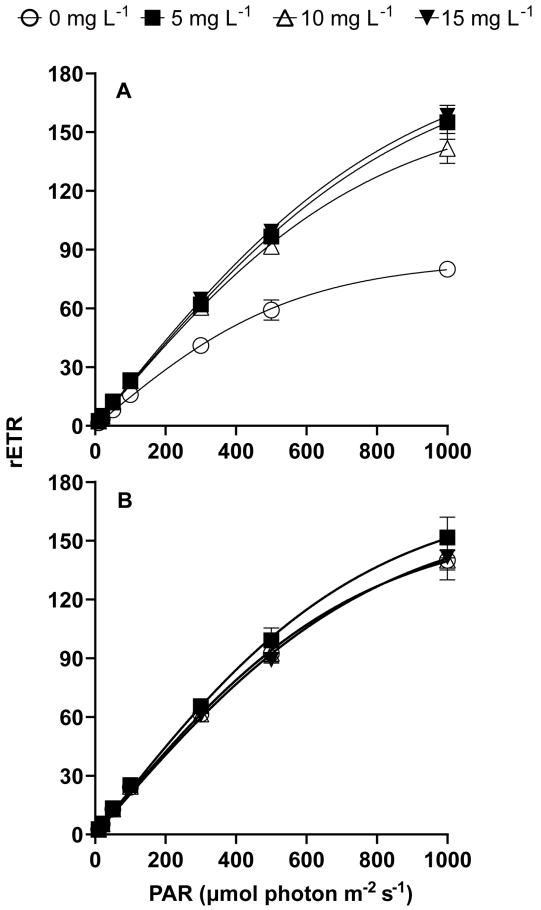

FIGURE 4
Relative electron transfer rate (rETR) of *P. donghaiense* under different NPs and CO_2 treatments at day 7. **(A)** LC, **(B)** HC. Lines represent the fit following a hyperbolic tangent function [Y = $rETR_{max}$ × tanh (α × X/$rETR_{max}$) (R^2 > 0.99, p< 0.001)]. Error bars represent the standard deviation of the mean of biological triplicates.

estimated. Compared to LC (LC0), HC (without NPs) improved F_v/F_m and Area but reduced V_I, V_J, M_0, and S_m (Figure 5). Moreover, energy transfer efficiency parameters showed an increase in response to HC, including the maximum quantum yield of primary photochemistry (φ_{P0}), the efficiency of a trapped exciton to move downstream (ψ_0), and the probability of an absorbed photon to move downstream (φ_{E0}) (Figure 5). The parameters related to the energy flux in the reaction center indicated a decrease in response to HC, such as absorption (ABS/RC), trapping (TR_0/RC), and dissipation energy (DI_0/RC) per active reaction center (RC), and an increase in transport energy (ET_0/RC). Furthermore, HC increased the density of the active reaction centers (RC/CS_0), absorption (ABS/CS_0), trapping (TR_0/CS_0), transport energy (ET_0/CS_0) per excited cross section (CS_0) and photosynthetic capacity (PI_{ABS}), but decreased the dissipation energy (DI_0/CS_0), significantly (Figures 5, 6).

In LC-treated *P. donghaiense*, NPs increased the F_v/F_m, φ_{P0}, ψ_0, φ_{E0}, ET_0/RC, ET_0/CS_0, and PI_{ABS}, but decreased the V_I, V_J, M_0, Area, S_m, ABS/RC, TR_0/RC, DI_0/RC, ABS/CS_0, TR_0/CS_0, DI_0/CS_0 (Figures 5, 6). However, in contrast to LC treatments, NPs enhanced the Area, RC/CS_0, and TR_0/CS_0 in HC treatments (Figure 5).

4 Discussion

4.1 The effect of NPs on *P. donghaiense*

The presence of NPs had a significant detrimental effect on the growth of *P. donghaiense* (Figure 1), which was attributed to NP-induced oxidative stress, consistent with previous studies (Natarajan et al., 2020; Sendra et al., 2019; Wang et al., 2021). SOD is an enzyme intricately linked to cellular oxygen metabolism in living organisms and protects organisms against oxidative stress. MDA is a critical byproduct of lipid peroxidation and is widely recognized as an indicator of cellular oxidative damage (Dong et al., 2020). Caro can eliminate excess ROS and inhibit lipid peroxidation (Rezayian et al., 2019), and the Caro/Chl-a ratio is a valuable indicator of non-enzymatic antioxidant capacity. In this study, NP-induced oxidative stress increased MDA levels, but the antioxidant mechanisms (SOD and Caro/Chl-a) were not enhanced (Figures 2C, 3). Therefore, NPs inhibited growth in the LC treatments due to the oxidative stress.

The variations in the physiological state of *P. donghaiense* cells in the presence of NPs were evident in the levels of Chl-a, rETR, and OJIP. Chl-a is crucial for energy capture and transfer during

10.3389/fmars.2024.1494930

TABLE 3 The fitted parameters derived from the rapid light curves (RLC) of *P. donghaiense* under different NPs and CO_2 concentrations.

Treatments		α	$rETR_{max}$	E_k ($rETR_{max}/\alpha$)
CO_2	NPs (mg L^{-1})			
LC	0	0.15 ± 0.02^{d}	85.00 ± 1.56^{c}	560.28 ± 10.25^{d}
	5	0.22 ± 0.00^{bc}	192.23 ± 15.90^{a}	893.56 ± 73.93^{a}
	10	0.21 ± 0.00^{bc}	166.23 ± 12.87^{b}	789.46 ± 61.12^{bc}
	15	0.22 ± 0.00^{ab}	193.77 ± 4.93^{a}	873.09 ± 22.22^{ab}
HC	0	0.22 ± 0.01^{abc}	159.77 ± 6.13^{b}	739.66 ± 28.38^{c}
	5	0.23 ± 0.01^{a}	175.40 ± 12.64^{ab}	765.60 ± 55.17^{c}
	10	0.22 ± 0.00^{abc}	159.67 ± 12.82^{b}	737.94 ± 59.25^{c}
	15	0.21 ± 0.01^{c}	166.67 ± 5.36^{b}	802.44 ± 25.79^{abc}

α, the initial slope of the RLC (μmol electrons m^{-2} s^{-1} (μmol photons m^{-2} s^{-1}) $^{-1}$); $rETR_{max}$, the maximum relative electron transfer rate (μmol electrons m^{-2} s^{-1}); and E_k, light saturation point (μmol photons m^{-2} s^{-1}). The data presented are the mean ± SD. One-way ANOVA (LSD test) results among the treatments are indicated by superscript letters, and the different superscripts indicate significant differences ($p < 0.05$, $n = 3$).

photosynthesis (Kato et al., 2020), and its increased content can compensate for growth by promoting photosynthesis (Figure 2A). This phenomenon is one of the adaptive mechanisms of microalgae in response to external stress (e.g., NPs) (Chen et al., 2022). $rETR_{max}$ can convert absorbed light energy into chemical energy that flows into the Calvin cycle, and α means photosynthetic efficiency at sub-saturating irradiance (Raniello et al., 2006). The rise in $rETR_{max}$ and α also implied that the stress response in cells increased photosynthesis under the NPs stress (Table 3). Chlorophyll fluorescence transient analysis (OJIP) provides insights into several photosynthetic parameters. In the LC-treated cells, the slope of the OJIP curve increased significantly with NPs treatment, indicating that the reduction in Q_A was rapid and that *P. donghaiense* responded vigorously to mitigate the effects of NPs (Chen et al., 2022) (Supplementary Figure S3A). ABS/RC, TR_0/RC, and ET_0/RC indicate the efficiency of light absorption, electron trapping, and

FIGURE 5
The heatmap of changes in the OJIP parameter values of *P. donghaiense* under different NPs and CO_2 treatments at day 7. Scale (right legend) indicates the level of positive (red, value > 1) or negative (blue, value< 1) correlation compared with the LC0. The value (φ_{E0} in LC5, 6.55) exceeding the maximum of the visible scale is represented by another deep red. LC0: LC without NPs; LC5: LC+5 mg L^{-1} NPs; LC10: LC+10 mg L^{-1} NPs; LC15: LC+15 mg L^{-1}NPs; HC0: HC without NPs; HC5: HC+5 mg L^{-1} NPs; HC10: HC+10 mg L^{-1} NPs; HC15: HC+15 mg L^{-1}NPs. The physiological meanings of parameters are shown in Supplementary Table S1.

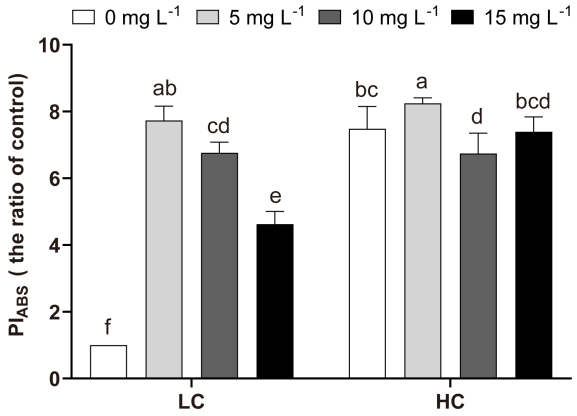

FIGURE 6
Variations in PI_{ABS} of *P. donghaiense* under different NPs and CO_2 treatments at day 7. One-way ANOVA (LSD test) results among the treatments are indicated by the letters over the bars, and different letters indicate significant differences among treatments ($p< 0.05$). Error bars represent the standard deviation of the mean of biological triplicates.

electron transport per reaction center, respectively. In contrast, DI_0/RC indicates the heat dissipation per reaction center (Rai-Kalal and Jajoo, 2021). Under NPs stress, the decrease of ABS/RC and TR_0/RC but an increase of ET_0/RC in LC treatments represented an improvement in the overall photochemical efficiency of primary photochemistry at the PSII reaction center of *P. donghaiense*, which is also manifested in the elevated levels of φ_{P0} (TR_0/ABS), ψ_0 (ET_0/TR_0) and φ_{E0} (ET_0/ABS) (Figures 5, 7). This might be attributed to the decrease in DI_0/RC, which minimized the energy loss by heat dissipation per reaction center, thereby increasing the photochemical efficiency of primary photochemistry in the presence of NPs (Figures 5, 7). PI_{ABS} is considered a sensitive and insightful indicator of stress and is widely used to compare primary photochemical reactions. Under NP-induced stress, PI_{ABS} increased significantly, suggesting a notable enhancement in the photosynthetic capacity of PSII (Figure 6). Although these changes reflected the stress response of cells to NPs under LC treatment, they did not alleviate NP-induced oxidative stress; therefore, the growth of *P. donghaiense* was significantly inhibited by NPs. Similarly, the diatom *P. tricornutum* also exhibited a stress response to improve photosynthesis, as reflected in the OJIP parameters and elevated Chl-a content when exposed to MPs (Chen et al., 2022). However, the response of microalgae to NPs is species-specific. The growth of the cyanobacteria *M. aeruginosa* was promoted by NPs owing to their strong antioxidant capacity and increased metabolic activity (Wang et al., 2023b).

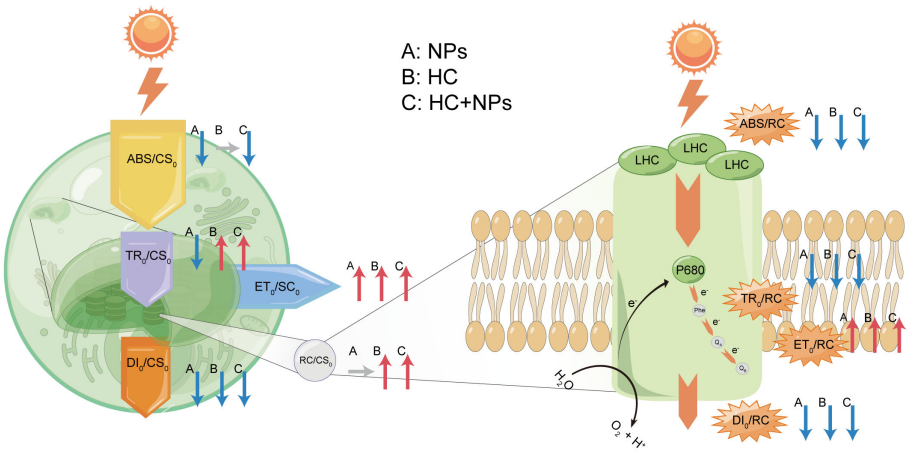

FIGURE 7
The energy pipeline models for phenomenological fluxes (per CS_0) (left) and the energy pipeline models for specific fluxes (per RC) (right). A: NPs, B: HC, C: HC+NPs. Red arrows signify an increase, blue arrows represent a decrease, and gray arrows indicate no difference. ABS/RC: Absorption per reaction center; TR_0/RC: Trapping per reaction center; ET_0/RC: electron transport per reaction center; DI_0/RC: Dissipation per reaction center; RC/CS_0: Density of the active reaction centers per cross-section; ABS/CS_0: Absorption per cross-section; TR_0/CS_0: Trapping per cross-section; ET_0/CS_0: Electron transport per cross-section; DI_0/CS_0: Dissipation per cross-section.

4.2 The effect of OA on *P. donghaiense*

The accelerated growth of *P. donghaiense* under OA (indicated by HC) conditions could be attributed to enhanced photosynthesis. The photosynthetic capacity (PI_{ABS}), photochemical efficiency (φ_{P0}, $\psi_{0,}$ and φ_{E0}), and photosynthetic efficiency (α) were all enhanced by HC compared with their efficiency under LC treatment, respectively (Figures 5, 6, Table 3). The increase in the number of active reaction centers (RC/CS_0) enhanced the efficient transfer of the maximum absorbed light energy to these centers (Figures 5, 7). This increase can be attributed to improved association between light harvesting center II (LHC II) and the PSII complex, resulting in enhanced electron flow from Q_A to Q_B in response to HC (Rai-Kalal and Jajoo, 2021). The significantly increased TR_0/CS_0 and ET_0/CS_0 under HC suggested a heightened energy flux per cross-section available for photosynthesis. This phenomenon may be attributed to a decrease in heat dissipation (DI_0/CS_0), which improved the efficiency of photosynthetic energy utilization (Figures 5, 7). The enhanced $rETR_{max}$ more effectively converted the absorbed light energy into chemical energy that flowed into the Calvin cycle (Table 3). Furthermore, HC decreases the allocation of electron transport to photorespiration and increases electron flow to Rubisco carboxylation, improving the efficiency of carbon concentration mechanisms (CCMs) (Robredo et al., 2010). The HC allows for 20% energy savings through downregulation of the CCMs (Hopkinson et al., 2011; Shi et al., 2015), which is expected to further stimulate growth (Fu et al., 2008; Ou et al., 2017) (Figure 1A) and photosynthetic rate (Chen et al., 2015; Dason et al., 2004; Wang et al., 2023c) (Figures 4, 6, 7).

4.3 The combined effect of OA and NPs on *P. donghaiense*

OA (HC) not only enhanced growth but also mitigated the adverse effects of NPs on *P. donghaiense* (Figure 1). Higher growth and less NP-induced inhibition were observed in the HC+NPs than in the LC+NPs (Figure 1). Under HC conditions, the heightened photosynthetic activity provided substantial energy to the cells, facilitating the functioning of the antioxidant system and thereby alleviating the oxidative stress induced by NPs (Ren et al., 2023), as indicated by increased SOD activity and decreased MDA content (Figure 3). Therefore, the cells maintained internal homeostasis, which was reflected in the relatively minor variations in OJIP parameters (Figure 5) and PI_{ABS} (Figure 6) compared with these parameters in LC. The unaltered parameters of α, $rETR_{max}$, φ_{P0}, $\psi_{0,}$ and φ_{E0} (Table 3, Figure 5) in HC treatment indicated that, in the presence of adequate cellular energy, the energy transfer efficiency did not display compensatory increments in photosynthesis under NPs, which was contradictory to the situation observed under LC. Similarly, OA can enhance the antioxidant capacity of microalgae to alleviate the adverse effects of environmental pollutants, such as cadmium (Dong et al., 2020), copper (Xu et al., 2022), and CuO (Wang et al., 2023a).

Under the impacts of climate change (e.g., OA) and environmental pollution (e.g., NPs), the occurrence of HAB has increased worldwide. Over the last two decades (2003–2020), the global extent of areas affected by blooms expanded by 13.2% (3.97 million km^2), and the frequency of global bloom outbreaks increased by 59.2% (Dai et al., 2023). Considering the Pacific coast of East Asia, including Chinese coastal waters, HAB have a significant deleterious influence on aquaculture and the ecological environment (Sakamoto et al., 2021; Yu et al., 2023). Since 1980, approximately 1622 algal blooms have been recorded in Chinese coastal waters (Sakamoto et al., 2021), with a growth rate of 40 ± 4% per decade (Xiao et al., 2019). Furthermore, climate change and environmental pollutants have a combined effect on HAB. OA alleviated the NPs-induced adverse effects and even completely diminished the inhibitory effects of NPs at $\leq 1 \times 10^{13}$ NP particles L^{-1}. The concentrations of NPs used in the experiments are much higher than those found in the natural environment, such as those in the Southern China Sea (about 2.2 items L^{-1}) and the northern Gulf of Mexico (74 items L^{-1}) (Wang et al., 2022). If these data are extrapolated to natural conditions, the effects of NPs on HAB in future OA scenarios can be disregarded as long as the NPs do not have more than 1×10^{13} particles L^{-1}. It can be assumed that HAB species can continuously bloom and threaten coastal communities and public health under future ocean conditions.

5 Conclusion

This study reveals the response of the HAB species *P. donghaiense* to NPs under OA conditions. NPs inhibited the growth of *P. donghaiense* by inducing oxidative stress, whereas OA promoted cell growth and alleviated NP-induced inhibitory effects by enhancing photosynthetic capacity. Therefore, this study provided a new insight that the combined effect of OA and NPs may promote the formation of HAB in future environments, thereby posing adverse impacts on marine ecosystems and public health.

Data availability statement

The original contributions presented in the study are included in the article/Supplementary Material. Further inquiries can be directed to the corresponding authors.

Author contributions

YZ: Writing – review & editing, Writing – original draft, Visualization, Validation, Supervision, Software, Resources, Project administration, Methodology, Investigation, Formal

analysis, Data curation, Conceptualization. QL: Writing – review & editing, Software, Project administration, Methodology, Investigation, Data curation. YY: Writing – review & editing, Supervision, Project administration, Methodology, Investigation, Data curation. YX: Writing – review & editing, Writing – original draft, Validation, Supervision, Resources, Project administration, Data curation. HC: Writing – review & editing, Software, Investigation, Data curation, Conceptualization. XF: Writing – review & editing, Visualization, Software, Project administration, Investigation. RG: Writing – review & editing, Writing – original draft, Software, Investigation, Funding acquisition, Conceptualization. WG: Writing – review & editing, Writing – original draft, Supervision, Resources, Project administration, Methodology, Investigation, Funding acquisition, Formal analysis, Data curation, Conceptualization.

Funding

The author(s) declare financial support was received for the research, authorship, and/or publication of this article. This research was supported by Zhejiang Provincial Natural Science Foundation of China under Grant No. ZCLY24D0601, the Research Program of Wenzhou Science & Technology Bureau No. N20220007, the Key Discipline of Zhejiang Province in Medical Technology (First Class, Category A). RG received funding from CONICET (PIP11220150100706) and FONCyT (PICT 2018-03992).

Acknowledgments

The image drawing process was supported by Figdraw. Furthermore, we would like to thank the reviewers whose comments and suggestions helped improve this manuscript.

Conflict of interest

The authors declare that the research was conducted in the absence of any commercial or financial relationships that could be construed as a potential conflict of interest.

Publisher's note

Supplementary material

The Supplementary Material for this article can be found online at: https://www.frontiersin.org/articles/10.3389/fmars.2024.1494930/full#supplementary-material

References

Anderson, D. M., Cembella, A. D., and Hallegraeff, G. M. (2012). Progress in understanding harmful algal blooms: paradigm shifts and new technologies for research, monitoring, and management. *Annu. Rev. Mar. Sci.* 4, 143–176. doi: 10.1146/annurev-marine-120308-081121

Badylak, S., Phlips, E., Batich, C., Jackson, M., and Wachnicka, A. (2021). Polystyrene microplastic contamination versus microplankton abundances in two lagoons of the Florida Keys. *Sci. Rep.* 11, 6029. doi: 10.1038/s41598-021-85388-y

Bausch, A. R., Juhl, A. R., Donaher, N. A., and Cockshutt, A. M. (2019). Combined effects of simulated acidification and hypoxia on the harmful dinoflagellate *Amphidinium carterae*. *Mar. Biol.* 166, 80. doi: 10.1007/s00227-019-3528-y

Besseling, E., Redondo-Hasselerharm, P., Foekema, E. M., and Koelmans, A. A. (2019). Quantifying ecological risks of aquatic micro- and nanoplastic. *Crit. Rev. Environ. Sci. Technol.* 49, 32–80. doi: 10.1080/10643389.2018.1531688

Brandenburg, K. M., Velthuis, M., and Van de Waal, D. B. (2019). Meta-analysis reveals enhanced growth of marine harmful algae from temperate regions with warming and elevated CO_2 levels. *Glob. Change Biol.* 25, 2607–2618. doi: 10.1111/gcb.14678

Chen, H., Guan, W., Zeng, G., Li, P., and Chen, S. (2015). Alleviation of solar ultraviolet radiation (UVR)-induced photoinhibition in diatom *Chaetoceros curvisetus* by ocean acidification. *J. Mar. Biol. Assoc. U. K.* 95, 661–667. doi: 10.1017/S0025315414001568

Chen, Z., Li, L., Hao, L., Hong, Y., and Wang, W. (2022). Hormesis-like growth and photosynthetic physiology of marine diatom *Phaeodactylum tricornutumBohlin* exposed to polystyrene microplastics. *Front. Environ. Sci. Eng.* 16, 13. doi: 10.1007/s11783-021-1436-0

Dai, Y., Yang, S., Zhao, D., Hu, C., Xu, W., Anderson, D. M., et al. (2023). Coastal phytoplankton blooms expand and intensify in the 21st century. *Nature* 615, 280–28+. doi: 10.1038/s41586-023-05760-y

Dason, J. S., Emma Huertas, I., and Colman, B. (2004). SOURCE OF INORGANIC CARBON FOR PHOTOSYNTHESIS IN TWO MARINE DINOFLAGELLATES1: SOURCE OF ci FOR DINOFLAGELLATES. *J. Phycol.* 40, 285–292. doi: 10.1111/j.1529-8817.2004.03123.x

Dong, F., Wang, P., Qian, W., Tang, X., Zhu, X., Wang, Z., et al. (2020). Mitigation effects of CO_2-driven ocean acidification on Cd toxicity to the marine diatom *Skeletonema costatum*. *Environ. pollut.* 259, 113850. doi: 10.1016/j.envpol.2019.113850

Feng, L.-J., Sun, X.-D., Zhu, F.-P., Feng, Y., Duan, J.-L., Xiao, F., et al. (2020). Nanoplastics promote microcystin synthesis and release from cyanobacterial microcystis aeruginosa. *Environ. Sci. Technol.* 54, 3386–3394. doi: 10.1021/acs.est.9b06085

Fu, F.-X., Zhang, Y., Warner, M. E., Feng, Y., Sun, J., and Hutchins, D. A. (2008). A comparison of future increased CO_2 and temperature effects on sympatric *Heterosigma akashiwo* and *Prorocentrum minimum*. *Harmful. Algae.* 7, 76–90. doi: 10.1016/j.hal.2007.05.006

Gao, G., Zhao, X., Jiang, M., and Gao, L. (2021). Impacts of marine heatwaves on algal structure and carbon sequestration in conjunction with ocean warming and acidification. *Front. Mar. Sci.* 8. doi: 10.3389/fmars.2021.758651

Gattuso, J.-P., Magnan, A., Billé, R., Cheung, W. W. L., Howes, E. L., Joos, F., et al. (2015). Contrasting futures for ocean and society from different anthropogenic CO_2 emissions scenarios. *Science* 349, aac4722. doi: 10.1126/science.aac4722

Gobler, C. J. (2020). Climate change and harmful algal blooms: insights and perspective. *Harmful. Algae.* 91, 101731. doi: 10.1016/j.hal.2019.101731

Guan, W., Si, R., Li, X., Cai, J., and Chen, S. (2018). Interactive effect of nitrogen source and high CO_2 concentration on the growth of the dinoflagellate *Alexandrium tamarense* and its toxicity to zebrafish (*Danio rerio*) embryos. *Mar. pollut. Bull.* 133, 626–635. doi: 10.1016/j.marpolbul.2018.06.024

Guillard, R. R. L., and Ryther, J. H. (1962). STUDIES OF MARINE PLANKTONIC DIATOMS: I. CYCLOTELLA NANA HUSTEDT, AND DETONULA CONFERVACEA (CLEVE) GRAN. *Can. J. Microbiol.* 8, 229–239. doi: 10.1139/m62-029

Hallegraeff, G., Enevoldsen, H., and Zingone, A. (2021). Global harmful algal bloom status reporting. *Harmful. Algae.* 102, 101992. doi: 10.1016/j.hal.2021.101992

Hopkinson, B. M., Dupont, C. L., Allen, A. E., and Morel, F. M. M. (2011). Efficiency of the CO_2-concentrating mechanism of diatoms. *Proc. Natl. Acad. Sci. U. S. A.* 108, 3830–3837. doi: 10.1073/pnas.1018062108

IPCC (2014). *Climate change 2014: synthesis Report. Contribution of Working Groups I, II and III to the Fifth Assessment Report of the Intergovernmental Panel on Climate Change*. Eds. Core Writing Team,, R. K. Pachauri and L. A. Meyer (Geneva, Switzerland: IPCC).

Jassby, A. D., and Platt, T. (1976). Mathematical formulation of the relationship between photosynthesis and light for phytoplankton. *Limnol. Oceanogr.* 21, 540–547. doi: 10.4319/lo.1976.21.4.0540

Jiao, Y., Zhu, Y., Chen, M., Wan, L., Zhao, Y., Gao, J., et al. (2022). The humic acid-like substances released from Microcystis aeruginosa contribute to defending against smaller-sized microplastics. *Chemosphere* 303, 135034. doi: 10.1016/j.chemosphere.2022.135034

Kang, B., Pecl, G. T., Lin, L., Sun, P., Zhang, P., Li, Y., et al. (2021). Climate change impacts on China's marine ecosystems. *Rev. Fish. Biol. Fish.* 31, 599–629. doi: 10.1007/s11160-021-09668-6

Kato, K., Shinoda, T., Nagao, R., Akimoto, S., Suzuki, T., Dohmae, N., et al. (2020). Structural basis for the adaptation and function of chlorophyll f in photosystem I. *Nat. Commun.* 11, 238. doi: 10.1038/s41467-019-13898-5

Lewis, E. R., and Wallace, D. W. R. (1998). *Program developed for CO_2 system calculation. Carbon Dioxide Information Analysis Center* (Tennessee: Lockheed Martin Energy Research Corporation for the US Department of Energy).

Lian, Z., Li, F., He, X., Chen, J., and Yu, R.-C. (2022). Rising CO_2 will increase toxicity of marine dinoflagellate *Alexandrium minutum*. *J. Hazard. Mater.* 431, 128627. doi: 10.1016/j.jhazmat.2022.128627

Liu, C., Qiu, J., Tang, Z., Hu, H., Meng, F., and Li, A. (2021). Effects of polystyrene microplastics on growth and toxin production of alexandrium pacificum. *Toxins* 13, 293. doi: 10.3390/toxins13040293

Lu, S., Ou, L., Dai, X., Cui, L., Dong, Y., Wang, P., et al. (2022). An overview of *Prorocentrum donghaiense* blooms in China: Species identification, occurrences, ecological consequences, and factors regulating prevalence. *Harmful. Algae.* 114, 102207. doi: 10.1016/j.hal.2022.102207

Nam, S.-H., Lee, J., and An, Y.-J. (2022). Towards understanding the impact of plastics on freshwater and marine microalgae: A review of the mechanisms and toxicity endpoints. *J. Hazard. Mater.* 423, 127174. doi: 10.1016/j.jhazmat.2021.127174

Natarajan, L., Omer, S., Jetly, N., Jenifer, M. A., Chandrasekaran, N., Suraishkumar, G. K., et al. (2020). Eco-corona formation lessens the toxic effects of polystyrene nanoplastics towards marine microalgae Chlorella sp. *Environ. Res.* 188, 109842. doi: 10.1016/j.envres.2020.109842

Niu, Z., Vandegehuchte, M. B., Catarino, A. I., and Everaert, G. (2021). Environmentally relevant concentrations and sizes of microplastic do not impede marine diatom growth. *J. Hazard. Mater.* 409, 124460. doi: 10.1016/j.jhazmat.2020.124460

Ou, G., Wang, H., Si, R., and Guan, W. (2017). The dinoflagellate *Akashiwo sanGuinea* will benefit from future climate change: The interactive effects of ocean acidification, warming and high irradiance on photophysiology and hemolytic activity. *Harmful. Algae.* 68, 118–127. doi: 10.1016/j.hal.2017.08.003

Porra, R. J. (2002). The chequered history of the development and use of simultaneous equations for the accurate determination of chlorophylls a and b. *Photosynth. Res.* 73, 149–156. doi: 10.1023/A:1020470224740

Qi, D., Ouyang, Z., Chen, L., Wu, Y., Lei, R., Chen, B., et al. (2022). Climate change drives rapid decadal acidification in the Arctic Ocean from 1994 to 2020. *Science* 377, 1544–1550. doi: 10.1126/science.abo0383

Qin, H., Sandrini, G., Piel, T., Slot, P. C., Huisman, J., and Visser, P. M. (2023). The harmful cyanobacterium Microcystis aeruginosa PCC7806 is more resistant to hydrogen peroxide at elevated CO2. *Harmful. Algae.* 128, 102482. doi: 10.1016/j.hal.2023.102482

Rai-Kalal, P., and Jajoo, A. (2021). Priming with zinc oxide nanoparticles improve germination and photosynthetic performance in wheat. *Plant Physiol. Biochem.* 160, 341–351. doi: 10.1016/j.plaphy.2021.01.032

Raniello, R., Lorenti, M., Brunet, C., and Buia, M. C. (2006). Photoacclimation of the invasive alga *Caulerpa racemosa* var. *cylindracea* to depth and daylight patterns and a putative new role for siphonaxanthin. *Mar. Ecol.- Evol. Perspect.* 27, 20–30. doi: 10.1111/j.1439-0485.2006.00080.x

Raven, J. A., Gobler, C. J., and Hansen, P. J. (2020). Dynamic CO_2 and pH levels in coastal, estuarine, and inland waters: Theoretical and observed effects on harmful algal blooms. *Harmful. Algae.* 91, 101594. doi: 10.1016/j.hal.2019.03.012

Ren, Y., Jia, Z., Liu, Y., Liang, C., Zhang, X., Xu, D., et al. (2023). Elevated pCO_2 alleviates the toxic effects of polystyrene nanoparticles on the marine microalga *Nannochloropsis oceanica*. Sci. *Total. Environ.* 895, 164985. doi: 10.1016/j.scitotenv.2023.164985

Rezayian, M., Niknam, V., and Ebrahimzadeh, H. (2019). Oxidative damage and antioxidative system in algae. *Toxicol. Rep.* 6, 1309–1313. doi: 10.1016/j.toxrep.2019.10.001

Riebesell, U., Aberle-Malzahn, N., Achterberg, E. P., Alguero-Muniz, M., Alvarez-Fernandez, S., Aristegui, J., et al. (2018). Toxic algal bloom induced by ocean acidification disrupts the pelagic food web. *Nat. Clim. Change* 8, 1082–108+. doi: 10.1038/s41558-018-0344-1

Robredo, A., Perez-Lopez, U., Lacuesta, M., Mena-Petite, A., and Munoz-Rueda, A. (2010). Influence of water stress on photosynthetic characteristics in barley plants under ambient and elevated CO_2 concentrations. *Biol. Plant* 54, 285–292. doi: 10.1007/s10535-010-0050-y

Rowenczyk, L., Leflaive, J., Clergeaud, F., Minet, A., Ferriol, J., Gauthier, L., et al. (2021). Heteroaggregates of polystyrene nanospheres and organic matter: preparation, characterization and evaluation of their toxicity to algae in environmentally relevant conditions. *Nanomater. Basel. Switz.* 11, 482. doi: 10.3390/nano11020482

Sakamoto, S., Lim, W. A., Lu, D., Dai, X., Orlova, T., and Iwataki, M. (2021). Harmful algal blooms and associated fisheries damage in East Asia: Current status and trends in China, Japan, Korea and Russia. *Harmful. Algae.* 102, 101787. doi: 10.1016/j.hal.2020.101787

Sendra, M., Staffieri, E., Yeste, M. P., Moreno-Garrido, I., Gatica, J. M., Corsi, I., et al. (2019). Are the primary characteristics of polystyrene nanoplastics responsible for toxicity and ad/absorption in the marine diatom Phaeodactylum tricornutum? *Environ. pollut. Barking. Essex. 1987* 249, 610–619. doi: 10.1016/j.envpol.2019.03.047

Sha, J., Xiong, H., Li, C., Lu, Z., Zhang, J., Zhong, H., et al. (2021). Harmful algal blooms and their eco-environmental indication. *Chemosphere* 274, 129912. doi: 10.1016/j.chemosphere.2021.129912

Shi, D., Li, W., Hopkinson, B. M., Hong, H., Li, D., Kao, S.-J., et al. (2015). Interactive effects of light, nitrogen source, and carbon dioxide on energy metabolism in the diatom *Thalassiosira pseudonana*. *Limnol. Oceanogr.* 60, 1805–1822. doi: 10.1002/lno.10134

Strasser, R. J., and Govindjee, (1992). "The fo and the O-J-I-P fluorescence rise in higher plants and algae," in *Argyroudi-Akoyunoglou, J.H. (Ed.), Regulation of Chloroplast Biogenesis* (Springer US, Boston, MA), 423–426. doi: 10.1007/978-1-4615-3366-5_60

Strasser, R. J., Srivastava, A., and Tsimilli-Michael, M. (2000). "The fluorescence transient as a tool to characterize and screen photosynthetic samples." in *Probing Photosynthesis: Mechanism, Regulation and Adaptation*. 445–483.

Strickland, J. D. H., and Parsons, T. R. (1972). *A Practical Handbook of Seawater Analysis*, *2nd edition*. (Ottawa, Canada: Fisheries Research Board of Canada). doi: 10.25607/OBP-1791

Taucher, J., Bach, L. T., Prowe, A. E. F., Boxhammer, T., Kvale, K., and Riebesell, U. (2022). Enhanced silica export in a future ocean triggers global diatom decline. *Nature* 605, 696–700. doi: 10.1038/s41586-022-04687-0

Wan, J.-K., Chu, W.-L., Kok, Y.-Y., and Lee, C.-S. (2018). "Distribution of microplastics and nanoplastics in aquatic ecosystems and their impacts on aquatic organisms, with emphasis on microalgae." in *Reviews of Environmental Contamination and Toxicology, volume 246*. (Cham: Springer International Publishing), 133–158. doi: 10.1007/398_2018_14

Wang, H., Niu, X., Feng, X., Gonçalves, R. J., and Guan, W. (2019). Effects of ocean acidification and phosphate limitation on physiology and toxicity of the dinoflagellate *Karenia mikimotoi*. *Harmful. Algae.* 87, 101621. doi: 10.1016/j.hal.2019.101621

Wang, H., Zhao, Y., Yin, S., Dai, Y., Zhao, J., Wang, Z., et al. (2023a). Antagonism toxicity of CuO nanoparticles and mild ocean acidification to marine algae. *J. Hazard. Mater.* 448, 130857. doi: 10.1016/j.jhazmat.2023.130857

Wang, Q., Liu, W., Zeb, A., Lian, Y., Shi, R., Li, J., et al. (2023b). Toxicity effects of polystyrene nanoplastics and arsenite on Microcystis aeruginosa. *Sci. Total. Environ.* 874, 162496. doi: 10.1016/j.scitotenv.2023.162496

Wang, R., Meng, L., Hu, S., Gao, P., Wang, C., Chen, J., et al. (2023c). Acidification of seawater attenuates the allelopathic effects of Ulva pertusa on Karenia mikimotoi. *Environ. Sci. pollut. Res.* 30, 5973–5982. doi: 10.1007/s11356-022-22607-7

Wang, S., Gao, Z., Liu, F., Chen, S., and Liu, G. (2021). Effects of polystyrene and triphenyl phosphate on growth, photosynthesis and oxidative stress of Chaetoceros meülleri. *Sci. Total. Environ.* 797, 149180. doi: 10.1016/j.scitotenv.2021.149180

Wang, X., Zhu, L., Liu, K., and Li, D. (2022). Prevalence of microplastic fibers in the marginal sea water column off southeast China. *Sci. Total. Environ.* 804, 150138. doi: 10.1016/j.scitotenv.2021.150138

Wu, S., Mi, T., Zhen, Y., Yu, K., Wang, F., and Yu, Z. (2021). A Rise in ROS and EPS Production: New Insights into the *Trichodesmium erythraeum* Response to Ocean Acidification. *J. Phycol.* 57, 172–182. doi: 10.1111/jpy.13075

Xiao, X., Agustí, S., Pan, Y., Yu, Y., Li, K., Wu, J., et al. (2019). Warming amplifies the frequency of harmful algal blooms with eutrophication in chinese coastal waters. *Environ. Sci. Technol.* 53, 13031–13041. doi: 10.1021/acs.est.9b03726

Xiao, W., Liu, X., Irwin, A. J., Laws, E. A., Wang, L., Chen, B., et al. (2018). Warming and eutrophication combine to restructure diatoms and dinoflagellates. *Water Res.* 128, 206–216. doi: 10.1016/j.watres.2017.10.051

Xu, D., Huang, S., Fan, X., Zhang, X., Wang, Y., Wang, W., et al. (2022). Elevated CO_2 reduces copper accumulation and toxicity in the diatom *Thalassiosira pseudonana*. *Front. Microbiol.* 13. doi: 10.3389/fmicb.2022.1113388

Yang, Y., Guo, Y., O'Brien, A. M., Lins, T. F., Rochman, C. M., and Sinton, D. (2020). Biological responses to climate change and nanoplastics are altered in concert: full-factor screening reveals effects of multiple stressors on primary producers. *Environ. Sci. Technol.* 54, 2401–2410. doi: 10.1021/acs.est.9b07040

You, X., Cao, X., Zhang, X., Guo, J., and Sun, W. (2021). Unraveling individual and combined toxicity of nano/microplastics and ciprofloxacin to Synechocystis sp. at the cellular and molecular levels. *Environ. Int.* 157, 106842. doi: 10.1016/j.envint.2021.106842

Yu, Z., Tang, Y., and Gobler, C. J. (2023). Harmful Algal Blooms in China: History, recent expansion, current status, and future prospects. *Harmful. Algae.* 129, 102499. doi: 10.1016/j.hal.2023.102499

Zhang, J., Kong, L., Zhao, Y., Lin, Q., Huang, S., Jin, Y., et al. (2022a). Antagonistic and synergistic effects of warming and microplastics on microalgae: Case study of the red tide species *Prorocentrum donghaiense*. *Environ. pollut.* 307, 119515. doi: 10.1016/j.envpol.2022.119515

Zhang, J., Yang, Q., Liu, Q., Liu, S., Zhu, Y., Yao, J., et al. (2022b). The responses of harmful dinoflagellate Karenia mikimotoi to simulated ocean acidification at the transcriptional level. *Harmful. Algae.* 111, 102167. doi: 10.1016/j.hal.2021.102167

Zhang, Z., Zhuang, Y., Chen, H., Lu, S., Li, Y., Ge, R., et al. (2021). Effects of *Prorocentrum donghaiense* bloom on zooplankton functional groups in the coastal waters of the East China Sea. *Mar. pollut. Bull.* 172, 112878. doi: 10.1016/j.marpolbul.2021.112878

Zhou, Y., Yan, W., and Wei, W. (2021). Effect of sea surface temperature and precipitation on annual frequency of harmful algal blooms in the East China Sea over the past decades. *Environ. pollut.* 270, 116224. doi: 10.1016/j.envpol.2020.116224

Zhou, Z. X., Yu, R. C., and Zhou, M. J. (2022). Evolution of harmful algal blooms in the East China Sea under eutrophication and warming scenarios. *Water Res.* 221, 118807. doi: 10.1016/j.watres.2022.118807

Zhou, Y., Zhang, Y., Li, F., Tan, L., and Wang, J. (2017). Nutrients structure changes impact the competition and succession between diatom and dinoflagellate in the East China Sea. *Sci. Total. Environ.* 574, 499–508. doi: 10.1016/j.scitotenv.2016.09.092